PRINCIPLES OF AIR CURTAINS AND THE IMPACT OF MASS FLOW RATE ON THERMAL BARRIER EFFECTIVENESS

Petros Sklavounos

The Cooper Union for Advancement of Science and Art, New York, NY

ABSTRACT

This research investigates the fluid dynamics and thermal performance of air curtains as a solution for maintaining thermal barriers between adjacent rooms. Ansys Fluent simulations were conducted for three operational scenarios: (1) a high mass flow rate of 3 kg/s, (2) a low mass flow rate of 0.5 kg/s, and (3) no air curtain. Results show that the low mass flow rate achieved a modest reduction in the second room's temperature at steady state by 0.97°C (from 21.60°C to 20.63°C), compared to no air curtain. The high mass flow rate achieved a more substantial reduction of 2.35°C (to 19.25°C), indicating that higher flow rates are more effective at lowering temperatures in the second room. In the atmospheric boundary area (first room), the temperature dropped by only 0.97°C in the low-flow case (from 25.45°C to 24.48°C) and by 1.35°C in the high-flow case (to 24.10°C). These findings suggest that while low mass flow rates offer some degree of thermal separation, higher flow rates provide significantly better performance in maintaining thermal barriers. The optimal configuration, however, depends on the desired balance between energy consumption and temperature reduction, as values used in this study were placeholders based on averages and literature values.

1. INTRODUCTION

The movement of air through open doorways connecting two environments can lead to significant fluid exchange, driven primarily by wind forces or stack effects arising from temperature gradients. This exchange facilitates heat and moisture transfer while also introducing undesirable contaminants such as dust, odors, and pathogens, which can compromise indoor air quality and increase energy consumption for heating and cooling. In industrial and healthcare settings, such as production lines and hospitals, these exchanges pose risks of contamination and disease transmission, respectively [1]. Traditionally, physical barriers like sliding doors or plastic strips have been used to mitigate infiltration. However, these mechanical solutions impede traffic flow, making them unsuitable for high-traffic entrances, including those in commercial or industrial spaces. To address these challenges, air curtain devices (ACDs) have emerged as a non-obstructive alternative. These devices create an aerodynamic seal by generating a plane turbulent impinging jet (PTIJ) that forms a virtual barrier across a doorway, effectively separating two environments in terms of heat and mass transfer [2][3].

A foundational contribution to air curtain research was made by Hayes and Stoecker [4], who introduced the deflection modulus (D_m), a dimensionless parameter defined as the ratio of jet momentum flux to the transverse forces acting across the jet. This parameter serves as a critical metric for determining the stability and performance of air curtains in sealed environments. Building on this, subsequent research has focused on extending the applicability of air curtains to ventilated spaces, where additional complexities, such as neutral pressure levels and leaky enclosures, influence performance. The performance of an air curtain is often characterized using sealing effectiveness (E), which compares the suppression of buoyancy-driven fluid exchange with and without the device.This is defined as:

$$E = \frac{\dot{Q}_{OD} - \dot{Q}_{ACD}}{\dot{Q}_{OD}} = 1 - \frac{\dot{Q}_{ACD}}{\dot{Q}_{OD}} \tag{1}$$

where $\dot{Q}_{ACD}$ and $\dot{Q}_{OD}$ represent the volumetric exchange rates with and without the air curtain, respectively. Values of E close to 1 indicate high sealing effectiveness, whereas E=0 corresponds to an unprotected opening [5].

In practical applications, air curtains are employed in diverse configurations, including downward, upward, or sideward blowing, and may incorporate recirculation systems for increased efficiency. Their effectiveness depends on several factors, including jet momentum flux, nozzle geometry, discharge angle, and environmental conditions such as temperature and pressure gradients [6]. For instance, a higher jet velocity may improve separation efficiency but can increase entrainment of ambient air, leading to diminishing returns in performance [7].

This study investigates the thermal and fluid dynamic behavior of air curtains by using computational fluid dynamics (CFD) for three operational scenarios: (1) high mass flow rate, (2) low mass flow rate, and (3) no air curtain. The goal is to provide

insights into the optimal operation of air curtains, balancing energy efficiency and performance requirements, as well as bridging knowledge gaps in this new fluid's application.

2. PROBLEM SETUP AND BOUNDARY CONDITIONS

2.1 Geometry and Domain

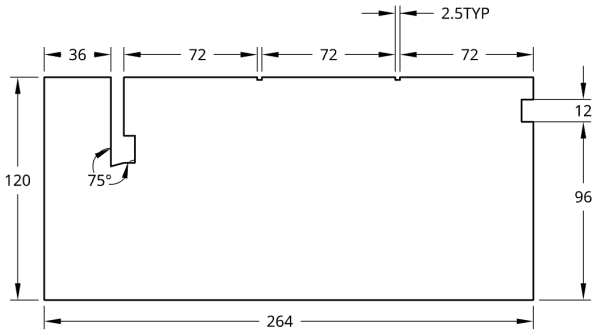

FIGURE 1: DIMENSIONED GEOMETRY OF ROOM LAYOUT

The system analyzed in this study consists of three primary regions: an atmospheric boundary on the left, a doorway equipped with an air curtain, indicated by the shorter floor-to-ceiling area, and a cooled room on the right. This can be seen in Figure 1 that has each feature dimensioned in inches. The overall domain measures 264in in length and 120in in height.

The atmospheric boundary represents the outdoor conditions and is located on the left side. It spans a width of 36in and allows for the introduction of natural airflow and thermal exchange into the system, which are critical for understanding the infiltration and exfiltration processes.

At the doorway, there is an air curtain designed to prevent heat and mass transfer between the atmospheric boundary and the cooled room. The nozzle discharges air at an angle of 15 degrees downward into the cooled room. This angle has been shown in prior studies to improve sealing efficiency by directing the jet flow toward the floor, thereby minimizing leakage and counteracting buoyancy-induced deflection. Such a configuration ensures that the air curtain effectively separates the two environments while allowing traffic through the doorway.

On the right side of the system is the cooled room to be separated from the ambient. This space is desired to be maintained at a stable temperature, where it has two ceiling-mounted recirculatory air conditioning inlets. These inlets are symmetrically spaced 72 cm apart and are designed to draw air from the room, cool it, and reintroduce it into the environment. The recirculation design ensures consistent thermal regulation, minimizing temperature gradients and reducing energy consumption compared to direct outlet systems. In terms of the setup for the CFD model, we will discuss in the next subsection how these components were defined.

2.2 Boundary Conditions

The computational model was configured to simulate the performance of the air curtain system under the three distinct cases of high mass flow rate, low mass flow rate, and of no air curtain operation. The boundary conditions were carefully selected to represent the physical system most accurately and to ensure numerical stability and convergence during simulations.These are shown visually in Figure 2, and explained in depth, component by component below.

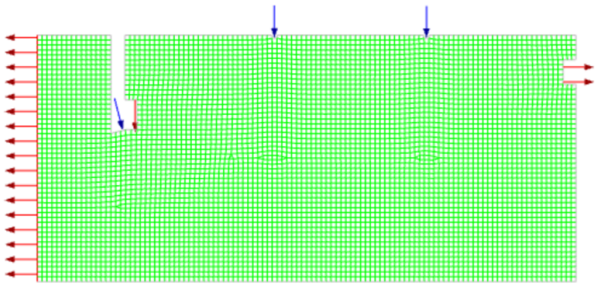

FIGURE 2: BOUNDARY CONDITIONS AND MESH OF DOMAIN

Air was modeled as an incompressible fluid with constant properties appropriate for room temperature conditions. The fluid properties used in the simulations are summarized in Table 1.

TABLE 1: FLUID PROPERTIES

Property	Value
Density (ρ)	1.225 kg/m^3
Specific Heat Capacity (c_p)	1006.43 $J/(kgK)$
Thermal Conductivity (k)	0.0242 $W/(mK)$
Viscosity (μ)	1.7894×10^{-5}kg/(m·s)
Molecular Weight (M)	28.966 kg/kmol

The boundary conditions applied to the various components of the model are detailed in Table 2 and Table 3 found below.

TABLE 2: BOUNDARY DEFINITION BY COMPONENT

Component	Boundary Type
Curtain Inlet	Recirculation Inlet
Inlet1	Recirculation Inlet
Inlet2	Recirculation Inlet
Curtain Outlet	Recirculation Outlet
Outlet	Recirculation Outlet
Atm Outlet	Pressure Outlet

TABLE 3: COMPONENT-SPECIFIC DETAILS

Component	Details
Curtain Outlet	Heat Source: 0 W
Inlet1	Heat Source: -3515 W
Inlet2	Heat Source: -3515 W
Curtain Inlet	3 kg/s (high), 0.5 kg/s (low), 0 kg/s (off)
Outlet	Recirculates air to match HVAC cooling requirements
Atm Outlet	Gauge Pressure: 0 Pa, Backflow Temp: 26.85°C

Air Curtain Mass Flow Rates: The mass flow rates for the curtain inlet were set to 3 kg/s for the high-flow scenario, 0.5 kg/s for the low-flow scenario, and 0 kg/s for the no air curtain case. These values were chosen to evaluate how different air curtain strengths influence thermal separation between the atmospheric boundary and the cooled room. Adjusting the mass flow rate highlights the relationship between the air curtain's momentum and its ability to reduce heat and mass transfer across the doorway.

Recirculation Outlets: Recirculation outlets were employed for the air conditioning inlet and the air curtain inlet. These outlets enable conditioned air to be drawn back into the system, enhancing energy efficiency and maintaining indoor temperature and air quality. Unlike velocity outlets, which assume a fixed flow direction, recirculation outlets better reflect the continuous operation of HVAC systems in buildings.

Inlets with Heat Source Specification: The air conditioning inlets (inlet_1 and inlet_2) and the air curtain inlet (curtain inlet) were modeled as recirculation inlets. (Inlet_1 and inlet_2) were assigned a heat source of -3515 W each to simulate the cooling effect of the air conditioning system.This value is from a typical cooling required BTU/hr for a room around $180 ft^2$ for commerical buildings. Using a heat source instead of fixed temperatures provides flexibility and more realism in representing the dynamic thermal loads, critical for capturing the system's performance under steady-state conditions.

Atmospheric Outlet Conditions: The atmospheric outlet (atmoutlet) was modeled as a pressure outlet with a gauge pressure of 0 Pa, simulating atmospheric conditions. This boundary allows air to freely enter or exit based on pressure and buoyancy forces. The backflow temperature was set to 26.85°C to match ambient conditions, with turbulence parameters consistent across all inlets and outlets.

Wall Conditions: All walls were modeled as stationary, adiabatic surfaces with a no-slip condition. The adiabatic assumption eliminates heat transfer through walls, as this is minimal as commerical building walls are typically insulated.Also this is negligible in magnitude. The no-slip condition ensures realistic interaction between the fluid and solid boundaries, capturing near-wall effects crucial for indoor flow dynamics.

Steady-State Simulation: The simulation was performed under steady-state conditions, reflecting the long operational timescales typical of building environments where HVAC systems operate continuously and over extended periods.

2.3 Simulation Parameters

The simulation was conducted using ANSYS Fluent in 2D, steady-state, double-precision mode to capture the detailed fluid flow and thermal interactions in the system. The steady-state approach best reflects the operational timescales of HVAC systems in buildings, where performance metrics are analyzed over extended period of times. A SST $k-\omega$ turbulence model was chosen for its accuracy in predicting boundary layer behavior and handling adverse pressure gradients. In this case this was critical for the interations of the recirculatory systems.

The governing equations included continuity, momentum, energy , and turbulence transport equations. Energy transfer was modeled to account for heat exchange between the air curtain, the ambient conditions of the outdoors, and the HVAC system. Overall, the SST $k-\omega$ model balances computational efficiency and precision for capturing the near wall effects present.

Numerical discretization was handled using second-order schemes for all equations, including pressure, momentum, turbulent kinetic energy, specific dissipation rate, and energy. This approach ensures higher accuracy and minimizes numerical diffusion, which is essential for resolving flow and thermal gradients. A coupled pressure-velocity coupling scheme was chosen to improve convergence for the steady-state solution.

The relaxation factors and limits set to avoid numerical divergence, such as the pressure, temperature, and turbulent parameters, were left to the default values.

3. RESULTS AND DISCUSSION

3.1 Computational Results

Case 1: High mass flow rate of 3 kg/s

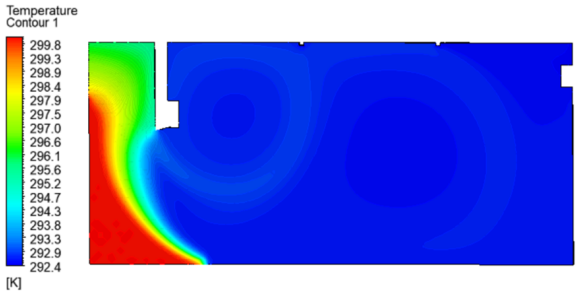

FIGURE 3: TEMPERATURE CONTOUR PLOT OF THE HIGH MASS FLOW AIR CURTAIN

The contour plot shows the temperature distribution within a domain, where:

- The left side contains warmer air, indicated by the red and green regions, corresponding to higher temperatures due to the ambient pressure opening on the left.
- The right side is shades of blue, representing colder temperatures maintained by an external cooling mechanism (e.g., air conditioning units).
- A curved transition zone exists between these regions, forming a thermal barrier created by the jet.

The jet emanates from the left side of the domain, exhibiting a steep temperature gradient transitioning from high to low temperatures (red to green). This gradient indicates:

- **High Initial Momentum:** The jet exits the nozzle with substantial energy, as evidenced by its ability to sustain a sharp temperature differential over a considerable distance.

- **Thermal Mixing Onset:** Limited diffusion occurs near the source, as the warmer region remains confined to the left side.

Jet Curvature and Seal Formation

The jet follows a curved trajectory, transitioning from the left to the center of the domain. This behavior is attributed to:

- **Cross-Jet Pressure Gradient:** A pressure differential across the jet induces curvature, forcing it to bend toward the cooler region.
- **Momentum Dominance:** The jet maintains its integrity over the curved path, suggesting a high momentum flux ratio (γ).

The curved profile serves as a thermal barrier, preventing significant mixing between the warm and cold regions. This behavior aligns with the reference study's observations at higher γ[3], where the jet creates an aerodynamic seal. The jet's curvature can be described by the following momentum equation:

$$\rho \frac{\partial \mathbf{u}}{\partial t} + \rho(\mathbf{u} \cdot \nabla)\mathbf{u} = -\nabla p + \mu \nabla^2 \mathbf{u}$$

where ρ is the density, $\mathbf{u}$ is the velocity vector, p is the pressure, and μ is the dynamic viscosity. The curvature arises from the interaction of momentum ($\rho(\mathbf{u} \cdot \nabla)\mathbf{u}$) and the pressure gradient ($-\nabla p$).

Thermal Separation Efficiency

The thermal separation efficiency is evidenced by the minimal penetration of warm air into the cold region. Unlike the reference study's Case c [3] ($\gamma = 9.07$), which exhibits significant mixing and entrainment.

Comparison with Reference Study

The observed flow field shares similarities with the reference study's Case c ($\gamma = 9.07$) in terms of jet curvature and penetration depth, but differs significantly in mixing and entrainment. It is important to note that in their setup, there were no AC units employed.The sharp temperature gradient in the contour plot indicates a more effective thermal seal compared to the reference study's high-γ cases, where entrainment reduces separation efficiency.

Figure 4 shows streamlines overlaying the temperature contour plot, which displays the direction of the flow and emphasizes the fluid interactions of the cold and hot boundaries.A recirculation outlet acts as a pressure sink, facilitating mass conservation within the system since without an outlet, the air entering the system would accumulate, increasing the pressure until flow stagnation or unsteady recirculation occurs. This outlet prevents the buildup of excess pressure that could otherwise destabilize the flow field, ensuring a steady-state operation.

In the context of the air curtain and the atmospheric pressure opening, the outlet can reduce the recirculation of warm air by providing a designated path for the exit of air from the system. Without an outlet, stagnation zones and vortices are more likely to develop, as was seen in the preliminary iteration, earlier in the semester. These vortices can lead to entrainment of warmer atmospheric air into the cold zone, diminishing the effectiveness of the air curtain.

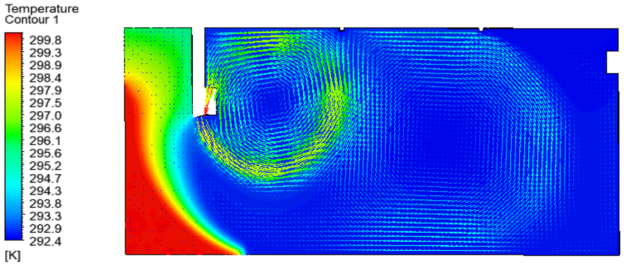

FIGURE 4: STREAMLINES OVERLAYING THE TEMPERATURE CONTOUR PLOT

Case 2: Low mass flow rate of 0.5 kg/s

The temperature contour shown in Figure 5 demonstrates moderate thermal separation, with the air curtain partially containing the warm air (red) in the left room while maintaining a cooler zone (blue) in the right room. However, the green and yellow regions near the interface indicate warm air infiltration into the cooler zone, suggesting reduced effectiveness compared to the higher flow rate case. In the high mass flow rate case, the air curtain successfully established a proper sealing depth, where the momentum flux (ρV^2) was sufficient to create a robust thermal barrier, effectively preventing warm air infiltration into the cooler zone. The higher velocity allowed the curtain to counteract cross-jet pressure gradients, penetrate deeply into the interface zone, and maintain aerodynamic stability. In contrast, the lower flow rate case lacks the necessary momentum to form an effective seal. The reduced momentum flux led to insufficient jet penetration and a weakened resistance to cross-flow pressure gradients, allowing the thermal barrier to break down and warm air to infiltrate. Additionally, the lower velocity increased the susceptibility to entrainment and turbulence at the interface, promoting mixing and compromising the separation. This can be attributed to a lower Reynolds number (Re $=\rho VD/\mu$), where inertial forces were insufficient to dominate over viscous forces, further weakening the jet's ability to maintain a cohesive seal. As a result, the lower flow rate case failed to achieve the thermal isolation seen in the high flow rate scenario, allowing significant thermal leakage and reducing energy efficiency.

Case 3: No mass flow rate of 0 kg/s

With this final case of no airflow, there is a drastic infiltration where all of the heat has infiltrated and is mixing with the cooler air. What is interesting is that the next AC inlet unit starts to act as an air curtain in itself. Understanding the change between all three cases is easiest when the geometry is split into the two rooms being discussed, where the first room is the entrance (atmospheric opening till air curtain nozzle), and the second room is the one past the nozzle with the AC units that we are trying to maintain a certain cool indoor temperature that is comfortable. Once this is done in ANSYS, the data can be post-processed for the mass-weighted average temperature of each room for steady-state. This

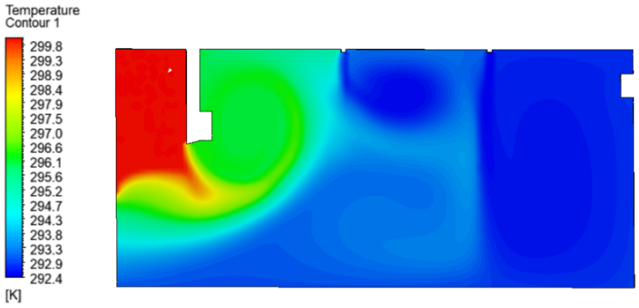

FIGURE 5: TEMPERATURE CONTOUR PLOT OF THE LOW MASS FLOW AIR CURTAIN

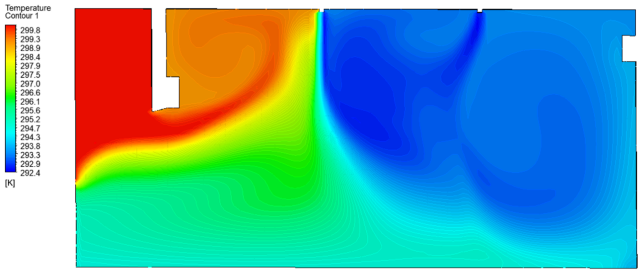

FIGURE 6: TEMPERATURE CONTOUR PLOT FOR NO MASS FLOW AIR CURTAIN

is shown in Table 4 and Table 5, whose only difference is units. To determine the average temperature for each room, the export case data is combined with a dictionary mapping IDs to mesh elements. Text recognition is employed to extract and list the mesh element IDs contained in each room, to then average their corresponding temperature values contained in the case data. This approach is used instead of a mass-weighted average area calculation because the rooms are not explicitly defined, and defining them on a surface proves challenging

TABLE 4: TEMPERATURES IN KELVIN FOR OFF, LOW, AND HIGH AIR CURTAIN CASES

Room	Off Case (K)	Low Case (K)	High Case (K)
1st Room	298.60	297.63	297.25
2nd Room	294.75	293.78	292.40

TABLE 5: TEMPERATURES IN CELSIUS FOR OFF, LOW, AND HIGH AIR CURTAIN CASES

Room	Off Case (°C)	Low Case (°C)	High Case (°C)
1st Room	25.45	24.48	24.10
2nd Room	21.60	20.63	19.25

In comparing the high and low mass flow cases, a key differentiator lies not just in the velocity and temperature fields, but also in the underlying turbulent structures and recirculation zones. At the higher mass flow rate, the stronger jet momentum creates a more stable shear layer at the interface between the warmer incoming air and the conditioned zone. This stability limits the formation of large-scale turbulent eddies and restricts the extent of recirculation zones near the doorway. As a result, the coherent and energetic jet flow better resists buoyancy-induced incursions, effectively minimizing infiltration and maintaining a sharper thermal gradient[4, 6, 7].

Conversely, in the low mass flow scenario, the reduced momentum of the jet weakens its ability to resist ambient turbulence. The lower Reynolds number flow leads to increased susceptibility to small-scale eddy formation and more pronounced recirculatory patterns. These recirculation zones facilitate the entrainment of warmer, ambient air into the cooled area, diluting the thermal barrier. Larger, more coherent vortical structures develop due to weaker velocity gradients, and these structures readily transport and mix higher-temperature fluid deeper into the conditioned space. Thus, the difference in turbulent structure and recirculation between the high and low flow cases provides an explanation for the increased infiltration observed at the lower mass flow rate, as the flow physics directly influence the jet's capacity to act as an effective aerodynamic and thermal barrier.

The analysis of the Low and High Cases for air curtain operation highlights a trade-off between energy efficiency and thermal performance. The High Case provides superior thermal separation, maintaining a larger temperature gradient (4.85°C) and minimizing warm air infiltration, making it ideal for scenarios where thermal comfort is critical. However, this comes at a significantly higher energy cost due to the cubic relationship between the air curtain mass flow rate and power consumption, derived from the fan affinity laws. According to these laws, the power required to drive a fan is proportional to the cube of the rotational speed (RPM), and since the volumetric flow rate (Q) is proportional to RPM, the power can be expressed as:

$$P \propto Q^3.$$

Using the relationship $\dot{m} = \rho Q$, where $\dot{m}$ is the mass flow rate and ρ is the air density (assumed constant), the fan power scales with the cube of the mass flow rate:

$$P \propto \dot{m}^3.$$

For the High Case ($\dot{m} = 3$ kg/s) and Low Case ($\dot{m} = 0.5$ kg/s), the ratio of power consumption becomes:

$$\frac{P_{\text{high}}}{P_{\text{low}}} = \left(\frac{\dot{m}_{\text{high}}}{\dot{m}_{\text{low}}}\right)^3 = \left(\frac{3}{0.5}\right)^3 = 216.$$

This explains why the High Case consumes substantially more energy. Over 12 hours of continuous operation, the High Case consumes approximately 540 kWh, costing \$81.00 at an electricity rate of \$0.15/kWh. In contrast, the Low Case consumes only 2.5 kWh, costing just \$0.38.

The performance difference corresponds to an improvement in the second room's thermal separation of approximately 1.38°C, with the High Case maintaining the second room at 19.25°C compared to 20.63°C for the Low Case. While the High Case achieves better thermal isolation, the energy cost is disproportionately higher due to the cubic scaling of fan power with mass

flow rate. This makes the High Case 213 times more expensive per degree Celsius of improvement in thermal separation.

For applications such as a lobby entrance in summer, where cost efficiency is important, the Low Case may be the better option, especially if we consider surcharge pricing practiced in NYC.

For verifying the magnitudes of temperature differences between the different rooms from the simulations, the temperature contour plots were replaced with an estimated value as a rectangle, and calculated manually shown in Figure 7 which is a quick and easy method.

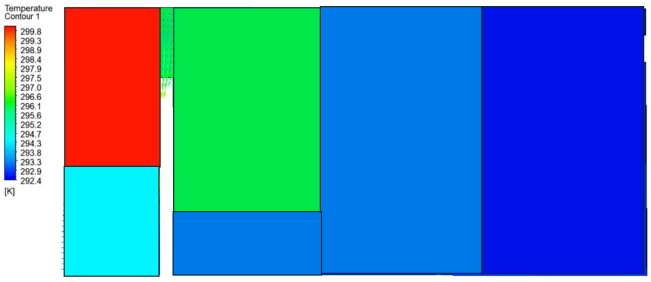

FIGURE 7: QUICK VERIFICATION OF ROOM TEMPERATURE AVERAGE TABLE VALUES

4. ANALYTICAL: GOVERNING EQUATIONS

To run this 'black box' computational model, various governing equations are used. The fluid flow and heat transfer are governed by the conservation laws of mass, momentum, and energy, coupled with appropriate turbulence modeling. We assume steady-state, incompressible flow and the Boussinesq approximation for buoyancy effects, which is valid for small density variations induced by temperature differences [6, 7].

4.1 Continuity (Mass Conservation)

For incompressible flow, the continuity equation is:

$$\nabla \cdot \mathbf{u} = 0, \tag{2}$$

where $\mathbf{u} = (u, v)$ is the velocity field. Mass conservation ensures that the inflow from the curtain nozzle and infiltration paths must be balanced by outflow through designated openings and recirculation outlets.

4.2 Momentum Equations (Navier-Stokes)

The steady-state momentum equations, under the Boussinesq approximation, are:

$$\rho(\mathbf{u} \cdot \nabla)\mathbf{u} = -\nabla p + \mu \nabla^2 \mathbf{u} + \rho \mathbf{g} \beta (T - T_{ref})\hat{\mathbf{y}}, \tag{3}$$

where:

- ρ is the reference fluid density,
- μ is the dynamic viscosity,
- $\mathbf{g}$ is gravitational acceleration (typically acting in the negative y-direction),
- β is the thermal expansion coefficient (with α being our more typical variable choice in Cooper courses), and
- T_{ref} is a reference temperature.

The buoyancy term $\rho g \beta (T - T_{ref})$ captures the density variations that drive natural convection. This is critical when assessing infiltration, as even slight temperature differences between the indoor and ambient air can lead to density gradients that influence flow directionality through openings.

4.3 Energy Equation

The steady-state energy equation (assuming no volumetric heat sources and negligible viscous dissipation) is:

$$\rho c_p (\mathbf{u} \cdot \nabla T) = \nabla \cdot (k \nabla T), \tag{4}$$

where c_p is the specific heat capacity and k is the thermal conductivity. This equation governs the temperature field, enabling the prediction of thermal gradients, heat infiltration, and the resulting efficiency of the air curtain.

4.4 Turbulence Modeling

To capture the complex mixing, recirculation, and shear layer dynamics of the air curtain, a two-equation turbulence model is employed. The Shear Stress Transport (SST) $k - \omega$ model is particularly suitable due to its accuracy in boundary layers and free shear flows and is what is used for the ANSYS Fluent simulations:

$$\frac{\partial(\rho k)}{\partial t} + \nabla \cdot (\rho k \mathbf{u}) = \nabla \cdot \left(\frac{\mu_t}{\sigma_k} \nabla k \right) + G_k - \rho \omega, \tag{5}$$

$$\frac{\partial(\rho \omega)}{\partial t} + \nabla \cdot (\rho \omega \mathbf{u}) = \nabla \cdot \left(\frac{\mu_t}{\sigma_\omega} \nabla \omega \right) + \alpha \frac{\rho G_k}{\mu_t} - \beta \rho \omega^2, \tag{6}$$

where k is the turbulent kinetic energy, ω is the specific dissipation rate, and μ_t is the turbulent viscosity. These equations ensure that the turbulent scales, production, and dissipation are well represented, allowing accurate prediction of jet behavior and recirculation.

5. DEFLECTION MODULUS AND JET STABILITY

A fundamental parameter for evaluating air curtain effectiveness is the Deflection Modulus (D_m):

$$D_m = \frac{\rho_0 b_0 u_0^2}{g h_b^2 (\rho_d - \rho_l)}, \tag{7}$$

where ρ_0 is the jet density, b_0 is the nozzle width, u_0 is the jet outlet velocity, and h_b is the height of the opening. The density difference $(\rho_d - \rho_l)$ and gravitational acceleration g appear in the denominator, reflecting the tendency of buoyancy forces to deflect or penetrate the jet. A higher D_m indicates that the momentum of the jet can effectively resist buoyancy-driven incursions, thus maintaining the sealing effectiveness. Literature often cites a critical minimum $D_{m,\min}$ around $1/8$ for stability; achieving values above this threshold ensures that the curtain remains intact and prevents significant infiltration.

6. HEAT TRANSFER AND THERMAL PERFORMANCE METRICS

Apart from the sealing effectiveness explored in Equation 1, a related measure is the heat transfer coefficient h, defined by:

$$h = \frac{Q}{b_0 h_b (T_l - T_d)}, \tag{8}$$

where T_l and T_d are representative temperatures on the lighter and denser fluid sides, respectively. Non-dimensional groupings like the Nusselt number (Nu), Reynolds number (Re), and Prandtl number (Pr) also arise in theoretical treatments, providing scaling relationships for convective heat transfer.

7. SAMPLE CALCULATION:DEFLECTION MODULUS CALCULATION FOR AIR CURTAIN STABILITY

This calculation includes the three cases of different mass flow rates and room temperatures. We also determine whether the calculated D_m is sufficient based on the literature threshold of $D_{m,\min} = 0.125$ [1, 5].

STEP-BY-STEP CALCULATION

Deflection Modulus Formula

$$D_m = \frac{\rho_0 b_0 u_0^2}{g h_b^2 (\rho_d - \rho_l)}$$

where:

- ρ_0: Density of air at the nozzle (approximated as the density of the 1st room)
- b_0: Nozzle width (7.424 in = 0.1886 m)
- u_0: Jet velocity (calculated from the mass flow rate)
- g: Gravitational acceleration (9.81 m/s^2)
- h_b: Height of the opening (72 in = 1.8288 m)
- ρ_d: Denser air density (2nd room)
- ρ_l: Lighter air density (1st room)

Air Density Calculation

Using the ideal gas law:

$$\rho = \frac{P}{RT},$$

where $P = 101325\,\text{Pa}$, $R = 287.05\,\text{J/(kg·K)}$, and $T\,(\text{in K}) = T_\text{C} + 273.15$:

- **Low Case** ($T_1 = 24.48°\text{C}$, $T_2 = 20.63°\text{C}$):

$$\rho_l = \frac{101325}{287.05 \cdot (24.48 + 273.15)} = 1.184\,\text{kg/m}^3,$$

$$\rho_d = \frac{101325}{287.05 \cdot (20.63 + 273.15)} = 1.201\,\text{kg/m}^3.$$

- **High Case** ($T_1 = 24.10°\text{C}$, $T_2 = 19.25°\text{C}$):

$$\rho_l = \frac{101325}{287.05 \cdot (24.10 + 273.15)} = 1.185\,\text{kg/m}^3,$$

$$\rho_d = \frac{101325}{287.05 \cdot (19.25 + 273.15)} = 1.205\,\text{kg/m}^3.$$

- **Free Flow Case** ($T_1 = 25.45°\text{C}$, $T_2 = 21.60°\text{C}$):

$$\rho_l = \frac{101325}{287.05 \cdot (25.45 + 273.15)} = 1.181\,\text{kg/m}^3,$$

$$\rho_d = \frac{101325}{287.05 \cdot (21.60 + 273.15)} = 1.197\,\text{kg/m}^3.$$

Jet Velocity Calculation

Assume the nozzle depth $d = 1\,\text{m}$. The simulation was 2D so this value is estimated. The jet velocity u_0 is:

$$u_0 = \frac{\dot{m}}{\rho_0 A_0}, \quad \text{where } A_0 = b_0 \cdot d.$$

- **Low Case:** For $\dot{m} = 0.5\,\text{kg/s}$,

$$u_0 = \frac{0.5}{1.184 \cdot 0.1886} = 2.22\,\text{m/s}.$$

- **High Case:** For $\dot{m} = 3\,\text{kg/s}$,

$$u_0 = \frac{3}{1.185 \cdot 0.1886} = 13.43\,\text{m/s}.$$

- **Free Flow Case:** $\dot{m} = 0\,\text{kg/s}$,

$$u_0 = 0\,\text{m/s}.$$

Deflection Modulus Calculation

$$D_m = \frac{\rho_0 b_0 u_0^2}{g h_b^2 (\rho_d - \rho_l)}$$

- **Low Case:**

$$D_m = \frac{1.184 \cdot 0.1886 \cdot (2.22)^2}{9.81 \cdot (1.8288)^2 (1.201 - 1.184)} = 0.183.$$

- **High Case:**

$$D_m = \frac{1.185 \cdot 0.1886 \cdot (13.43)^2}{9.81 \cdot (1.8288)^2 (1.205 - 1.185)} = 3.55.$$

- **Free Flow Case:**

$$D_m = 0.$$

Critical Minimum Velocity and Mass Flow Rate

To ensure $D_m \geq 0.125$:

$$u_\text{crit} = \sqrt{\frac{D_m \cdot g \cdot h_b^2 \cdot (\rho_d - \rho_l)}{\rho_0 b_0}}.$$

For the **Low Case**:

$$u_\text{crit} = \sqrt{\frac{0.125 \cdot 9.81 \cdot (1.8288)^2 \cdot (1.201 - 1.184)}{1.184 \cdot 0.1886}} = 1.91\,\text{m/s}.$$

The corresponding mass flow rate:

$$\dot{m} = \rho_0 A_0 u_\text{crit} = 1.184 \cdot 0.1886 \cdot 1.91 = 0.43\,\text{kg/s}.$$

Results Table

Case	u_0 (m/s)	D_m	ρ_l (kg/m^3)	ρ_d (kg/m^3)
Low Flow	2.22	0.183	1.184	1.201
High Flow	13.43	3.55	1.185	1.205
Free Flow	0.00	0.00	1.181	1.197

8. CONCLUSION

In summary, this study has demonstrated that properly implemented air curtains can significantly limit thermal infiltration between adjacent spaces, effectively creating an aerodynamic barrier that restricts warm air from entering cooler environments. Results indicate that while a higher mass flow rate (3 kg/s) can achieve superior temperature reductions and a more pronounced thermal gradient, it does so with a considerable increase in energy consumption. Conversely, a lower mass flow rate (0.5 kg/s) offers a more energy-efficient compromise, yielding a substantial reduction in infiltration at a fraction of the operational cost. These findings affirm the potential of air curtains to maintain desired thermal conditions, as highlighted in the abstract, and underscore the importance of balancing performance with cost and energy considerations. It is worth noting that although the low flow case had a Deflection modulus that was greater than the critical minimum of 0.125, its contour plot looked more like a Dm value of 0.05, shown in Agrawal,[5] which did not achieve complete sealing.This was likely due to the rough calculation of the velocity from the mass flow rate, which needed an area for the jet outlet and was likely overestimated due to the nozzle depth being a meter long.

Looking forward, future work could explore adaptive or variable-flow air curtains that dynamically adjust jet velocity and angle in response to changing environmental conditions. Investigations into alternative nozzle geometries, turbulence model refinements, and the incorporation of more complex boundary conditions, such as transient weather effects or occupant-induced drafts, may further enhance predictive accuracy. Additionally, experimental validation of these numerical findings, such as in Frank et al. [7], Agrawal et al. [5], and Ruiz et al.[6] would improve the quality of the dive into air curtains.

REFERENCES

[1] Kairo, Guillaume, Pioz, Maryline, Tchamitchian, Sylvie, Pelissier, Michel, Brunet, Jean-Luc and Belzunces, Luc P. "Efficiency of an air curtain as an anti-insect barrier: the honey bee as a model insect." *Pest Management Science* Vol. 74 No. 12 (2018): pp. 2707–2715. DOI 10.1002/ps.5090.

[2] ASHRAE, ASHRAE. "ASHRAE handbook-HVAC applications." *American Society of*. 2011.

[3] Khayrullina, Adelya, van Hooff, Twan, Alanis Ruiz, Claudio and van Heijst, GertJan. "Minimum momentum flux ratio required to prevent air curtain breakthrough in case of cross-curtain pressure gradients: CFD versus analytical equation." *Building Simulation* Vol. 13 (2020): pp. 943–960. DOI 10.1007/s12273-020-0633-2.

[4] Hayes, Floyd Corliss. "HEAT TRANSFER CHARACTERISTICS OF THE AIR CURTAIN: a PLANE JET SUBJECTED TO TRANSVERSE PRESSURE AND TEMPERATURE GRADIENTS." Ph.D. Thesis, University of Illinois at Urbana-Champaign. n.d. URL https://www.proquest.com/docview/302293781?fromopenview=true&fromunauthdoc=true&pq-origsite=gscholar&sourcetype=Dissertations%20&%20Theses. ProQuest Dissertations & Theses.

[5] Agrawal, Tanmay, Agarwal, Shresth, Chalamalla, V. K. and Jha, Narsing Kumar. "Performance and flow dynamics of heavy air curtains using experiments and numerical simulations." *Environmental Fluid Mechanics* Vol. 24 (2024): pp. 875–898. DOI 10.1007/s10652-023-09948-8.

[6] Ruiz, Claudio Alanis, Van Hooff, Twan, Blocken, Bert and Van Heijst, GertJan. "Air curtain performance: Introducing the adapted separation efficiency." *Building and Environment* Vol. 188 (2020): p. 107468. DOI 10.1016/j.buildenv.2020.107468.

[7] Frank, D. and Linden, P. F. "The effectiveness of an air curtain in the doorway of a ventilated building." *Journal of Fluid Mechanics* Vol. 756 (2014): pp. 130–164. DOI 10.1017/jfm.2014.433.

APPENDIX

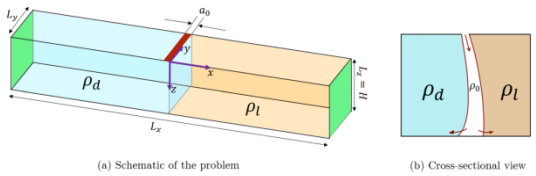

FIGURE 8: USEFUL GRAPHIC OF EXPERIMENTAL SETUP FROM AGRAWAL ET AL.[5]

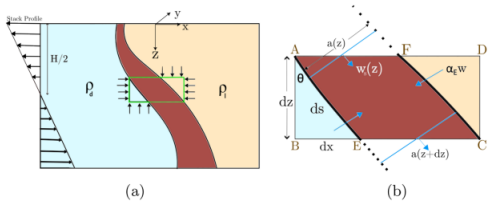

Fig. 3 Control volume chosen for the formulation of the analytical model

FIGURE 9: USEFUL GRAPHIC THAT WAS WELL DESCRIBED IN AGRAWAL ET AL.[5]